Hindawi
Advances in Materials Science and Engineering
Volume 2019, Article ID 6454087, 8 pages
https://doi.org/10.1155/2019/6454087

Research Article

Fabrication and Uniaxial Tensile Properties of Soldered Porous Copper Fiber-Sintered Sheets

Ruiliang Liu, Wei Zhou, Shuangli Li, and Dongsheng Xu

Department of Mechanical & Electrical Engineering, Xiamen University, Xiamen 361005, China

Correspondence should be addressed to Wei Zhou; abczhoulin@163.com

Received 16 December 2018; Revised 25 March 2019; Accepted 18 June 2019; Published 1 July 2019

Guest Editor: Shimaa El-Hadad

Porous copper fiber-sintered sheets (PCFSSs) with different porosities were fabricated through the solid-phase sintering method using cutting copper fibers. PCFSSs with the same porosity and different porosities were then joined via a fluxless soldering method. By analyzing the uniaxial tensile property of the PCFSSs, the formation mechanism of the soldered PCFSSs was investigated. The difference in the tensile properties between the soldered and original PCFSSs was examined. Experimental results indicated that, for the PCFSSs with homogeneous porosity, reducing the porosity increased the tensile strength and elongation at break significantly. The fluxless soldering method with the lead-free solder resulted in excellent joining of the PCFSSs with the same porosity and different porosities. Moreover, the final tensile strength of the soldered PCFSSs with the same porosity was nearly equal to that of their parent PCFSSs. The tensile strength of the soldered PCFSSs with different porosities depended on the higher-porosity section. After soldering the PCFSSs, Young's modulus increased and the elongation at break reduced.

1. Introduction

With the development of precision manufacturing and material processing technology, porous metal materials are attracting considerable interest from researchers as novel structural and functional materials. In particular, porous metal fiber-sintered sheets made of metal fibers have been used in many industrial applications, such as filtration and separation, energy absorption, and noise reduction, and have been used in microreactors, heat exchangers, fuel cells, etc. [1–7]. They have excellent structural properties because of their interconnected, three-dimensional (3D) network structure and have high porosities and large specific surface areas.

Porous copper fiber-sintered sheets (PCFSSs) are usually fabricated via the sintering method or the wet layup method [8]. The performance of PCFSSs is closely related to the fiber type, sintering process, pore size, etc. For example, Clyne and Markaki fabricated porous stainless steel fiber-sintered sheets via the liquid-phase sintering method with copper powder as the connecting agent. However, the tensile strength of the stainless steel fiber-sintered sheets in the porosity range of 75%–95% was no higher than 1 MPa [9–11]. Tang et al. fabricated stainless steel fiber felts via the solid-phase sintering method with 28 μm fibers and performed synchrotron radiation experiments to investigate the sintering mechanism and the evolution of the sintered neck, which significantly affect the mechanical strength [12, 13]. Zhou et al. used 100 μm cutting copper fibers to fabricate PCFSSs via the solid-phase sintering method and systematically studied the effects of the sintering conditions (including the sintering temperature and time), fiber distribution, and porosity on the tensile strength [14–16]. Liu et al. fabricated entangled steel wire materials with stainless steel fibers and investigated the pore structure, Young's modulus, and tensile strength of the materials. The tensile strength of a stainless steel porous material with 61.8% porosity was 40.1 MPa, and Young's modulus was as high as 2.7 GPa [17, 18]. Markaki and Clyne investigated the mechanical properties of porous metal fiber materials by performing a combined theoretical and numerical analysis [11, 19, 20].

Compared with porous metal fiber materials having homogeneous pore structures, porous metal materials with gradient pore structures, owing to their improved flow resistance and permeability, have exhibited better

performance in applications such as microreactors, sound absorption and noise reduction, and micro-heat exchangers [21]. For example, Zhou et al. used porous copper fiber-sintered felts with a gradient porosity as catalyst supports to design laminated-sheet methanol steam-reforming microreactors for hydrogen production. The porous copper fiber-sintered felts with three-grade porosity (70%-80%-90%) exhibited better methanol conversion and a high H_2 flow rate [22]. Meng et al. compared experimental and calculated results to show that porous metal fiber materials with gradient structures had a higher sound-absorption coefficient. In particular, when stringent restrictions were placed on the total volume and/or weight of the sound-absorbing material, the porous sound-absorbing materials with a gradient structure exhibited unparalleled performance advantages [23].

Several studies have indicated that methods such as gluing, riveting, welding, and soldering can be used to fabricate porous metal materials with gradient pore structures [24–31]. Ashby et al. [24] and Olurin [25] presented a feasible method for the soldering of aluminum foams with fluxes, and Huang et al. [26, 27] described fluxless soldering for connecting aluminum foam materials. However, the removal of oxide layers was necessary, and the strength of the joints was usually lower than that of their parent material. Recently, the connection of stainless steel foam materials and nickel foam materials has also attracted considerable attention.

In summary, porous metal materials with a gradient pore structure have exhibited significant advantages in many applications. However, the successful joining of porous metal fiber-sintered materials with a gradient pore structure has not been reported. In this study, cutting copper fibers were used to fabricate PCFSSs with homogeneous porosity. Subsequently, the PCFSSs were joined via a fluxless soldering method to form soldered PCFSSs with gradient pore structures. By analyzing the pore structure and uniaxial tensile properties of the soldered PCFSSs, the soldering formation mechanism of the PCFSSs was investigated. The difference in the tensile properties between the soldered and original PCFSSs was examined.

2. Experimental Procedures

2.1. Fabrication of PCFSSs. The fabrication process for PCFSSs with homogeneous porosity involves three stages: copper fiber cutting, fiber molding, and solid-phase sintering [32]. In this study, rough-surface copper fibers were fabricated via a cutting method on a common lathe using a multitooth tool. A 99.5% pure copper bar with a diameter of 40 mm was used as the workpiece material. Continuous copper fibers with an equivalent diameter of approximately 100 μm were obtained by adjusting the cutting parameters. Subsequently, the continuous copper fibers were cut into short fibers with lengths between 10 and 20 mm. The short fibers were evenly filled in a rectangular mold. A mold-pressing device was used to apply a specific pressure to the metal fibers. A bolt was then employed to tighten the pressure plate, producing a porous copper fiber sheet sample with the same shape as the mold. A box-type furnace in a gas-protection atmosphere (RXL-12-11) was used in the sintering process. The hydrogen gas pressure and the sintering temperature in the chamber were maintained at 0.3 MPa and 900°C, respectively. The heating rate and sintering time were set as 5°C/min and 30 min, respectively. The sintering process parameters are shown in Figure 1. When the sintering process was completed, PCFSSs with a specified shape were obtained, as shown in Figure 2. In this study, PCFSSs with two different shapes were fabricated, with dimensions of 100 mm × 15 mm × 4 mm and 50 mm × 15 mm × 4 mm. The porosities of the PCFSSs were 70%, 75%, 80%, 85%, and 90%. The mass-volume method was used to calculate the porosity of each PCFSS:

$$\varepsilon = \left(1 - \frac{m}{\rho V}\right) \times 100\%, \tag{1}$$

where ε represents the porosity of the PCFSS, m represents the mass of the copper fiber, ρ represents the density of copper, and V represents the volume of the PCFSS.

2.2. Fluxless Soldering for Joining PCFSSs. To avoid damage to the PCFSS pore structure due to the high temperatures or pressures produced by melt welding or pressure welding, we proposed a fluxless soldering method for the joining of PCFSSs with different porosities. A handheld electric iron (BuFan ABF203H, Dongguan, China) at a temperature of approximately 380°C was used as the heat source. The filler metal, a lead-free solder, was composed of 99.3 wt.% Sn, and its melting point was approximately 227°C. During the soldering process, a high-temperature iron head was used to stir the molten filler metal to keep the solder in the liquid phase and create a uniform coating. The molten solder was coated onto the surface of the PCFSSs and then quickly percolated into the pore structure under the action of capillary forces of the micropores. After cooling and solidification, a stable and reliable soldering joint was formed, and a soldering connection of PCFSSs with different porosities was achieved. In this study, two short sintering plates with dimensions of 50 mm × 15 mm × 4 mm were joined into a long sheet with dimensions of 100 mm × 15 mm × 4 mm. The soldering width of the molten filler metal coating on the joining surface was controlled to be 6–8 mm. The soldering process is illustrated in Figure 3.

2.3. Testing Microstructure and Mechanical Properties of PCFSSs. The surface morphology of the soldered PCFSSs was observed via scanning electron microscopy (SEM) (Hitachi SU-70, Japan), and a component analysis of the soldering joint was performed using energy-dispersive X-ray spectroscopy (EDX). The pore size (defined as the equivalent diameter of the interspaces between adjacent fibers) and pore-size distribution of the PCFSSs were measured using an image-analysis software (Nano Measurement) via the statistical method. Five viewpoints were chosen from the two-dimensional cross-sectional and longitudinal micromorphology images of each porous specimen. Tensile testing of

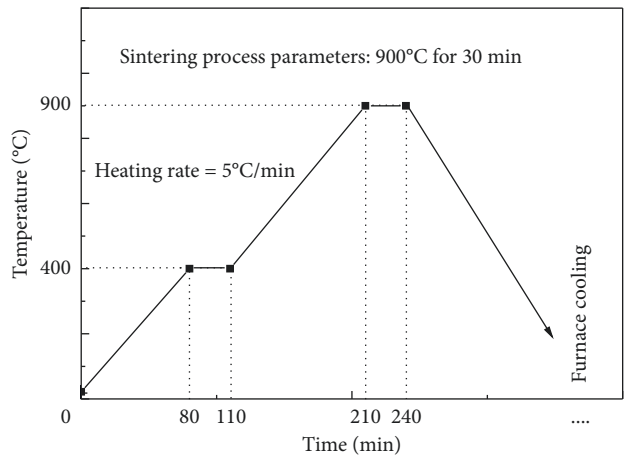

Figure 1: Parameters of the sintering process for the PCFSSs.

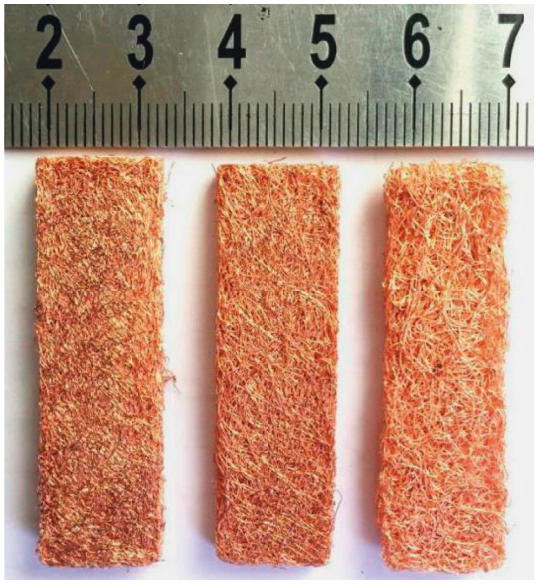

Figure 2: PCFSS samples: (a) $\varepsilon = 70\%$; (b) $\varepsilon = 80\%$; (c) $\varepsilon = 90\%$.

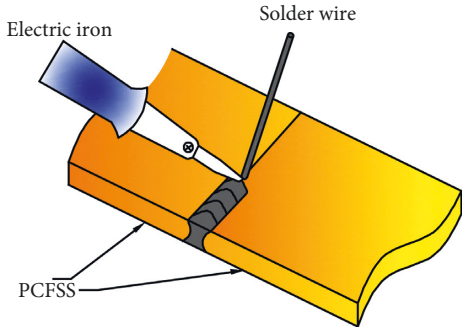

Figure 3: Schematic of the PCFSS soldering process.

the PCFSSs was performed using a desktop universal tension-testing machine (KS-M08, Dongguan, China). To satisfy the requirements for tensile testing, both the homogeneous-porosity PCFSSs and the soldered PCFSSs were set to the same size of 100 mm × 15 mm × 4 mm. The tensile-testing samples were clamped to ensure that the length of the effective testing region was 50 mm, and then the samples were pulled at a constant tensile rate of 10 mm/min. The tensile testing was performed at room temperature (approximately 25°C).

3. Results and Discussion

3.1. Microstructure Characteristics of PCFSSs. The pore-size distribution and surface morphology of PCFSSs with different porosities are shown in Figure 4. The copper fibers were in a disordered arrangement and formed a large number of 3D interconnected pores with random irregular shapes. This can be attributed to the random filling of copper fibers in the mold cavity. The filling and molding processes resulted in a 3D network structure with many contact points between the fibers. During the sintering process, the material migration between adjacent fibers was accelerated at a high temperature, and sintering joints were easily formed via metallurgy bonding. Further investigation revealed that two types of sintering joints were present in the PCFSSs: length-to-length contact joints and crossing fiber joints [33]. The cross mesh structure and the formation of sintering necks improved the mechanical strength of the PCFSSs, expanding their range of applications.

Figure 4 presents the pore-size distribution of PCFSSs with different porosities. The abscissa represents the pore-size range, and the ordinate represents the proportion of the pore-size range. As shown, the porosity significantly affected the pore-size distribution of the PCFSSs. PCFSS with 70% porosity had an average pore size of 169 μm, and 88.4% of the pores had a size <300 μm. PCFSSs with 80% and 90% porosities had average pore sizes of 213 and 242 μm, respectively. With an increase in the porosity from 70% to 90%, the maximum pore size increased from 634 to 775 μm, indicating that pore size was distributed over a wider range. Therefore, an inhomogeneous pore-size distribution was obtained for the PCFSSs with high porosities. Conversely, a lower porosity yielded a more centralized and uniform pore-size distribution.

3.2. Mechanism Analysis of PCFSS Soldering Joints. The appearance of the PCFSSs after soldering and the surface morphology of the soldering joint are shown in Figure 5. There was no apparent macroscopic structural damage near the soldering joint, owing to the relatively low temperature and pressure used during the soldering process. Additionally, the solder adhered to the copper fiber surfaces in the soldering area, forming a dense bonding layer (Figure 5(a)). The effectiveness of fluxless soldering depends on the wetting, spreading, and capillary flow of the molten solder [26]. During the soldering process, wetting of the solder on the PCFSS surface is required for solder spreading and capillary action. The internal capillary force of PCFSS micropores causes the molten solder to spread. The SEM images showed that the lead-free solder had good wettability on the PCFSS

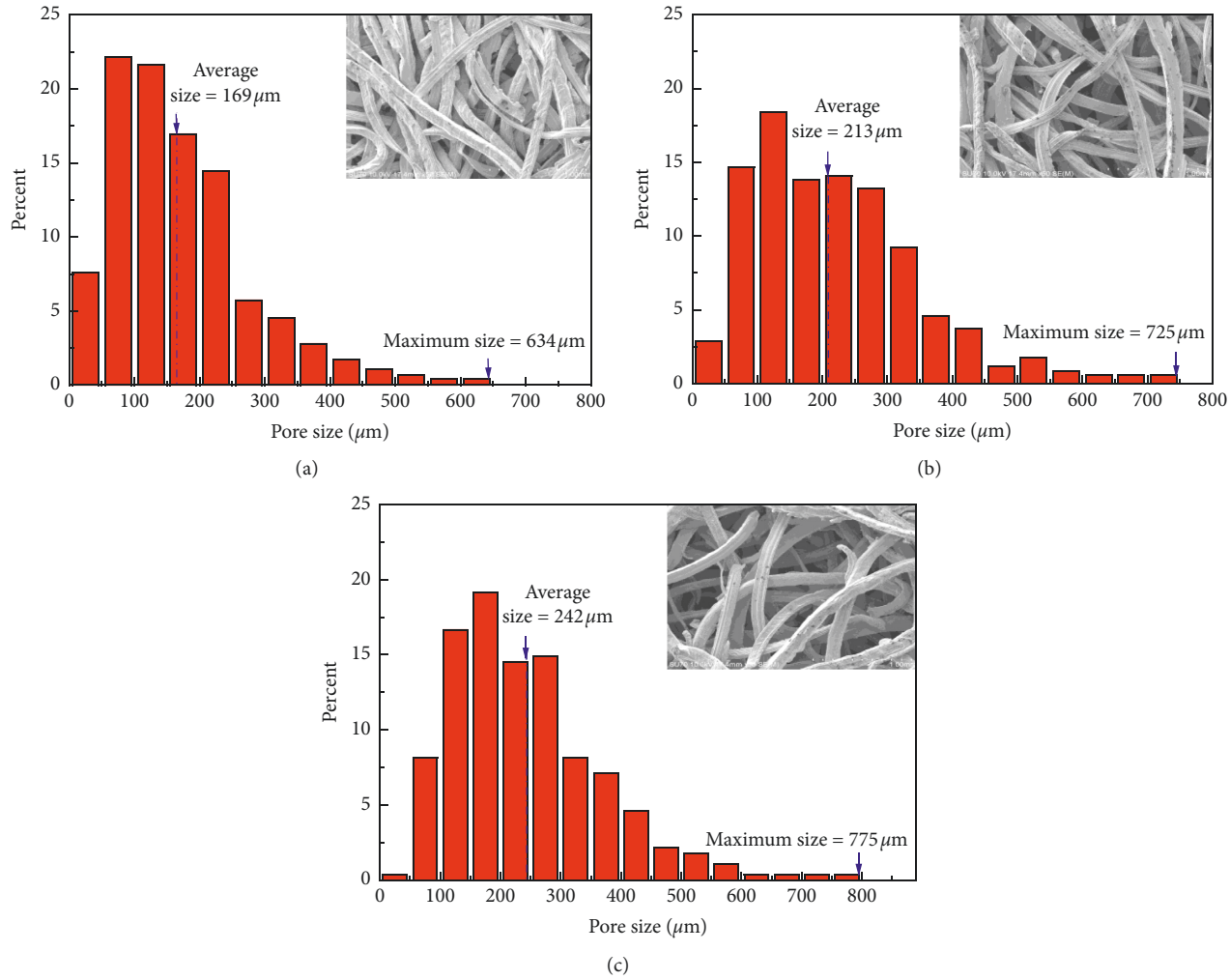

Figure 4: Surface morphology and pore-size distribution of PCFSSs with different porosities: (a) $\varepsilon = 70\%$; (b) $\varepsilon = 80\%$; (c) $\varepsilon = 90\%$.

surface, and the interconnected pore structure and rough fiber surface promoted the spreading of the filler metal into the PCFSS. Furthermore, there were no oxide layers appearing during the soldering process. Therefore, in contrast to the soldering of other dense materials or aluminum foam materials [34], the problems of oxide layers can be ignored; the filler metal easily spread to the soldering seam and filled the pore structure of the PCFSSs (Figures 5(b) and 5(c)).

Figure 5(d) presents the longitudinal profile along the tangent C-C in the PCFSS soldering joint (Figure 5(a)). As shown in Figure 5(a), uniform solder layers with a depth of approximately 1.5 mm existed on both the upper and lower surfaces of the PCFSS after soldering. The bond between the filler metal and the copper fibers was relatively dense, and no distinct defects existed. EDX was used to analyze the elemental components in different colored areas (Figure 5(e)). The results indicate that the components in light-gray phase A and dark-gray phase B were tin (99.13 wt.%) and copper (99.69 wt.%), respectively.

Figure 6 presents the results of the line-scan EDX analysis of the copper-solder interface. These results (shown in Figure 6) and the SEM image (Figure 5(e)) indicate that tin and copper were distributed continuously throughout the interfacial layer. Thus, the solder metal spread along the microscratches of copper fibers. The grain boundaries of the fibers were dissolved extensively, following which the alloy resolidified, forming a dendritic microstructure at the interface. This interdiffusion contributed to the bonding at the atomic scale. Notably, during the soldering process, the Sn solder not only achieved excellent wetting on the PCFSS surface but also permeated through the micropores. By forming a uniform and dense interface with the copper fibers, the soldering connection of the PCFSSs was finally realized.

3.3. Effects of Porosity on Tensile Properties of PCFSSs. The tension fracture of the PCFSSs resulted from the destruction of interfiber sintering joints and fiber breaking. If the fiber parameters and the sintering process are strictly controlled, porosity is the decisive factor that influences the number of fiber sintering joints and the tensile properties of PCFSSs. The uniaxial tensile stress-strain curves of PCFSSs

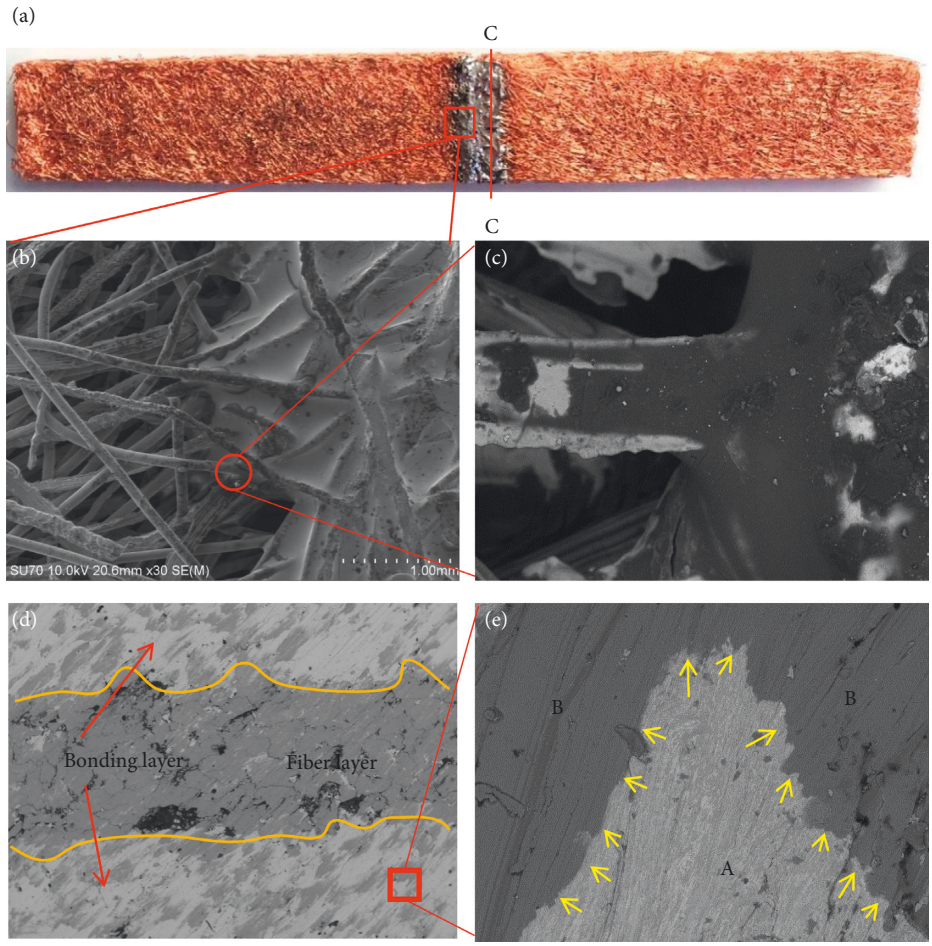

Figure 5: Appearance of soldered PCFSSs and surface morphology of the soldering joint.

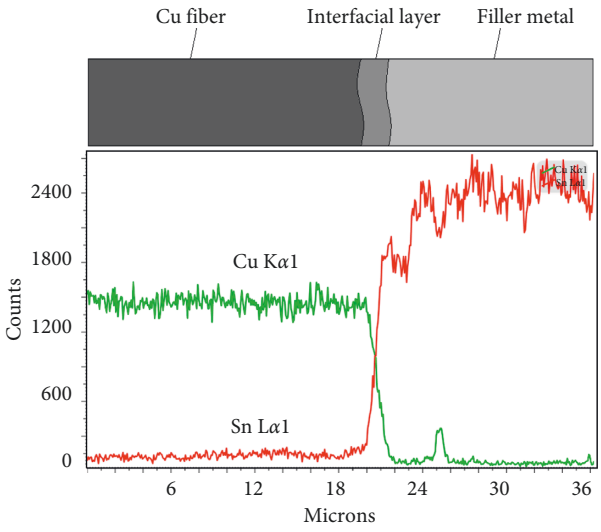

Figure 6: Line-scan EDX analysis of the interfacial area.

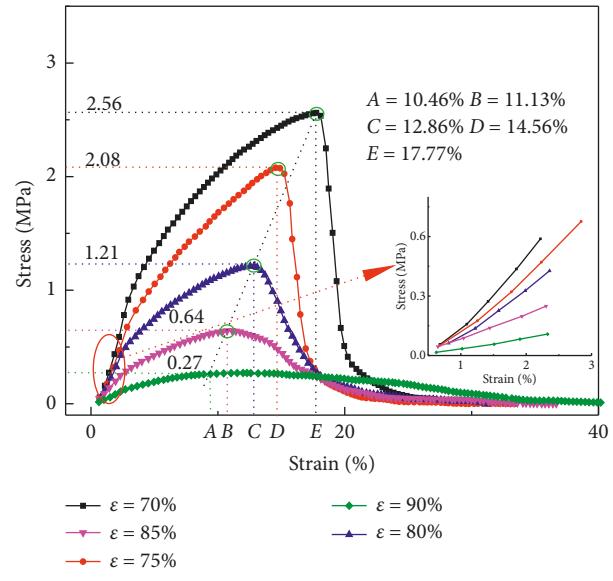

Figure 7: Uniaxial tensile stress-strain curves of PCFSSs with different porosities.

with different porosities are shown in Figure 7; here, the sample size was 100 mm × 15 mm × 4 mm. All the PCFSS samples experienced a rapid stage of linear elastic deformation in the initial tension process (illustrated in Figure 7 and its enlarged partial view). Then, without distinct yielding signs, the samples entered the plastic-deformation stage directly. With a further increase in the tension and strain, the stress reached the maximum value, and the testing

Figure 8: Tensile fracture appearance of soldered PCFSSs with the same porosity.

sample was broken. This was defined as the fracture stage [15, 17]. The tension fracture behavior of the PCFSSs was different from that of traditional plastic materials, including the linear-elastic stage, yielding stage, hardening stage, and necking stage. It was even different from that of ordinary brittle materials because of the prolonged plastic-deformation stage. Comparison of the stress-strain curves of PCFSSs with different porosities revealed that as the PCFSS porosity decreased, the tensile strength increased. When the porosity decreased from 90% to 70%, the tensile strength of the PCFSSs increased from 0.27 to 2.56 MPa. Additionally, as the porosity decreased, the elongation at break increased. In particular, the elongation at break of the PCFSS with 90% porosity was more than 5%. This indicates that PCFSSs with porosities in the 70–90% range possess good ductility. Obviously, the mechanical properties of PCFSSs are determined by their internal organization and structure. As the porosity decreased, more contact regions between the fibers existed in the PCFSS, which not only promoted the formation of sintering joints but also increased the bearing area [33]. These results provide a valuable reference for the design and manufacture of porous metal fiber materials with high strength.

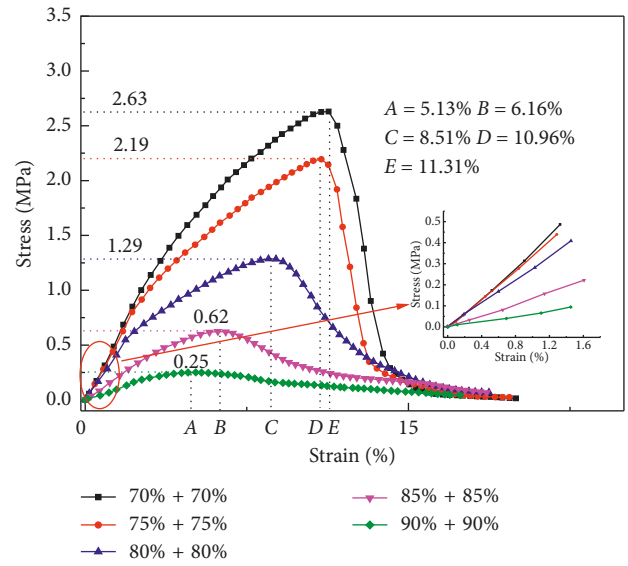

Figure 9: Uniaxial tensile stress-strain curves of soldered PCFSSs with the same porosity.

3.4. Uniaxial Tensile Performance of Soldered PCFSSs with the Same Porosity. Figure 8 shows the typical tensile fracture appearance of soldered PCFSSs with the same porosity. Clearly, the fracture occurred far from the soldering joint, suggesting that the tensile strength of the soldering joint was higher than that of the parent PCFSSs. As indicated by the uniaxial tensile stress-strain curves of the soldered PCFSSs with the same porosity (Figure 9), the tension process of the soldered PCFSSs can be divided into three typical stages: an elastic-deformation stage, a plastic-deformation stage, and a fracture stage. With the decreasing porosity, the tensile strength and the elongation at break increased for the soldered PCFSSs with the same porosity. These results agree with the conclusions drawn from the homogeneous-porosity PCFSS samples. Additionally, the change in the PCFSS tensile strength after soldering was negligible, but the elongation at break after soldering was significantly reduced. This is mainly because during the soldering process, the molten filler metal easily spread into the pore structure and formed a dense bonding layer. This increased the mechanical strength of the PCFSS at the bonding layer. However, it reduced the material ductility, and eventually, the elongation at break of the soldered PCFSS was reduced.

Compared with the other stages in the tensile process of the PCFSSs, the elastic-deformation stage was relatively short, and the stress-strain relationship for this stage satisfied Hooke's law for linear elasticity. Therefore, Young's modulus of the PCFSSs could be calculated according to the linear stress-strain relationship. The calculated values are shown in Figure 10. Young's moduli of the PCFSSs in the porosity range of 70%–90% were between 5.39 and 34.64 MPa. Young's modulus increased with the decreasing porosity.

A lower porosity of the PCFSS inevitably results in more fibers and sintered necks per unit volume and greater resistance to deformation under an impact load [33]. Young's modulus of the soldered PCFSSs ($E = 37.65$ MPa) with the same porosity ($k = 70\%$) was slightly higher than that of the parent PCFSSs ($E = 34.64$ MPa), indicating that the overall stiffness of the PCFSSs was slightly increased after soldering. This is mainly because the liquid solder permeated into the internal pore structure of the PCFSSs and then solidified into a compound material with the copper fibers. The solidified solder had a more compact structure than the PCFSSs [27]. Owing to the solidified soldered layer, the mechanical strength and Young's modulus of the sample increased simultaneously.

3.5. Uniaxial Tensile Strength of Soldered PCFSSs with Different Porosities. Figure 11 shows the uniaxial tensile stress-strain curves of soldered PCFSSs with different porosities.

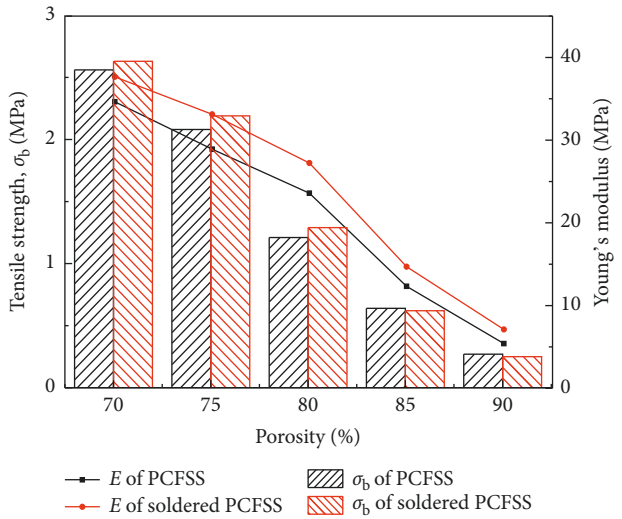

Figure 10: Comparison of the tensile properties of PCFSSs with homogeneous porosity and soldered PCFSSs with the same porosity.

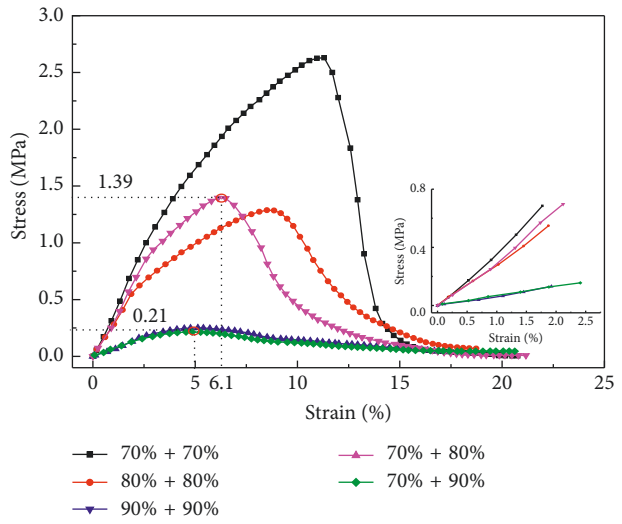

Figure 11: Uniaxial tensile stress-strain curves of soldered PCFSSs with different porosities.

The tensile strengths of the soldered PCFSSs with gradient-porosity types 70% + 80% and 70% + 90% were 1.39 and 0.21 MPa, respectively. The tensile strengths of the soldered PCFSSs with same-porosity types 80% + 80% and 90% + 90% were 1.29 and 0.25 MPa, respectively. As mentioned previously, the soldering joint of the soldered PCFSSs was strong enough to withstand the tensile load; thus, fracture did not occur in the joint area. When fracture was inevitable, naturally, the higher-porosity section with a lower tensile strength broke first. Therefore, the overall tensile strength of soldered PCFSSs with different porosities depended on the parent PCFSS with a higher porosity.

4. Conclusions

Cutting copper fibers were used as raw materials to fabricate PCFSSs with different porosities via the solid-phase sintering method. PCFSSs with the same porosity and different porosities were joined via a fluxless soldering method. For PCFSSs with a homogeneous porosity in the range of 70%–90%, the tensile strength and elongation at break increased significantly with the decreasing porosity. SEM and EDX indicated that the fluxless soldering method with the lead-free solder achieved excellent joining of the PCFSSs with the same porosity and different porosities without causing serious damage. The tensile strength of the soldered PCFSSs with the same porosity was no lower than that of their parent nonsoldered PCFSSs. The tensile strength of the soldered PCFSSs with different porosities depended on the higher-porosity section. Additionally, owing to the solidified soldered joint, Young's modulus of the soldered PCFSSs increased and the elongation at break decreased. The fluxless soldering method is feasible for joining porous metal fiber-sintered sheets and can play an important role in expanding the applications of porous metal fiber materials.

Data Availability

The photograph data used to support the findings of this study are all included within the article. The data are available to be accessed when needed.

Conflicts of Interest

The authors declare no conflicts of interest.

Authors' Contributions

Ruiliang Liu presented the method to fabricate soldered PCFSSs and measured their tensile strength. Wei Zhou gave some suggestions to design the soldered PCFSSs and wrote the paper. Shuangli Li provided the porous copper fiber-sintered sheets with different porosities. Dongsheng Xu helped to measure the tensile strength and collected experimental data.

Acknowledgments

This work was supported by the Guangdong Natural Science Funds for Distinguished Young Scholars (No. 2016A030306032), the Natural Science Foundation of Fujian Province of China (No. 2017J06015), and the Fundamental Research Funds for Central Universities, Xiamen University (No. 20720160079).

References

[1] I. Yuranov, L. Kiwi-Minsker, and A. Renken, "Structured combustion catalysts based on sintered metal fibre filters," *Applied Catalysis B: Environmental*, vol. 43, no. 3, pp. 217–227, 2003.

[2] Y. Tang, Z. He, M. Pan, Z. Wan, L. Lu, and L. Pan, "Fabrication and characterization of aluminum fibers by peripheral milling," *Materials and Manufacturing Processes*, vol. 25, no. 10, pp. 1052–1058, 2010.

[3] D. Chen, L. Hou, W. Zhou, and R. Liu, "Tri-dimensional reticulated porous material sintered by multi-tooth tool

cutting-made copper fibers and investigation of its acoustical performances," *Materials Letters*, vol. 194, pp. 9–12, 2017.

[4] A. Bedeloglu, N. Sunter, and Y. Bozkurt, "Manufacturing and properties of yarns containing metal wires," *Materials and Manufacturing Processes*, vol. 26, no. 11, pp. 1378–1382, 2011.

[5] W. Zhou, Y. Tang, M. Pan, X. Wei, H. Chen, and J. Xiang, "A performance study of methanol steam reforming microreactor with porous copper fiber sintered felt as catalyst support for fuel cells," *International Journal of Hydrogen Energy*, vol. 34, no. 24, pp. 9745–9753, 2009.

[6] W. Ling, W. Zhou, R. Liu, Q. Qiu, and J. Liu, "Thermal performance of loop heat pipe with porous copper fiber sintered sheet as wick structure," *Applied Thermal Engineering*, vol. 108, pp. 251–260, 2016.

[7] Y. Tang, W. Yuan, M. Pan, and Z. Wan, "Feasibility study of porous copper fiber sintered felt: a novel porous flow field in proton exchange membrane fuel cells," *International Journal of Hydrogen Energy*, vol. 35, no. 18, pp. 9661–9677, 2010.

[8] D. Das, B. S. Butola, and S. Renuka, "An investigation into fiber dispersion behavior in water with reference to Wet-Lay nonwoven technology," *Journal of Dispersion Science and Technology*, vol. 33, no. 8, pp. 1225–1232, 2012.

[9] T. Clyne, A. Markaki, and J. Tan, "Mechanical and magnetic properties of metal fibre networks, with and without a polymeric matrix," *Composites Science and Technology*, vol. 65, no. 15-16, pp. 2492–2499, 2005.

[10] A. Markaki, V. Gergely, and A. Cockburn, "Production of a highly porous material by liquid phase sintering of short ferritic stainless steel fibres and a preliminary study of its mechanical behaviour," *Composites Science and Technology*, vol. 63, no. 16, pp. 2345–2351, 2003.

[11] A. E. Markaki and T. W. Clyne, "Mechanics of thin ultra-light stainless steel sandwich sheet material," *Acta Materialia*, vol. 51, no. 5, pp. 1341–1350, 2003.

[12] A. Li, J. Ma, J. Wang, Z. Xu, C. Li, and H. Tang, "Sintering diagram for 316L stainless steel fibers," *Powder Technology*, vol. 288, pp. 109–116, 2016.

[13] J. Z. Wang, H. P. Tang, and M. Qian, "Fabrication of high strength and ductile stainless steel fiber felts by sintering," *Journal of Metals*, vol. 68, no. 3, pp. 1–9, 2016.

[14] B. Liu, X.-G. Wang, Y. Tang, W. Yuan, C.-B. Fang, and Z.-P. Wan, "Experimental study on the tensile property of a novel oriented linear porous metal," *Advances in Materials Science and Engineering*, vol. 2016, Article ID 3930703, 8 pages, 2016.

[15] C. Fang, Z. Wan, B. Liu, and L. Lu, "A novel sintered stainless steel fiber felt with rough surface morphologies," *Advances in Materials Science and Engineering*, vol. 2014, Article ID 546020, 7 pages, 2014.

[16] S. Zou, Z. Wan, L. Lu, and Y. Tang, "Experimental study on tensile properties of a novel porous metal fiber/powder sintered composite sheet," *Materials*, vol. 9, no. 9, p. 712, 2016.

[17] P. Liu, G. He, and L. Wu, "Uniaxial tensile stress-strain behavior of entangled steel wire material," *Materials Science and Engineering: A*, vol. 509, no. 1-2, pp. 69–75, 2009.

[18] P. Liu, G. He, and L. H. Wu, "Fabrication of sintered steel wire mesh and its compressive properties," *Materials Science and Engineering: A*, vol. 489, no. 1-2, pp. 21–28, 2008.

[19] M. Z. Jin, C. Q. Chen, and T. J. Lu, "The mechanical behavior of porous metal fiber sintered sheets," *Journal of Mechanics and Physics of Solids*, vol. 61, no. 1, pp. 161–174, 2013.

[20] P. S. Liu, "Mechanical behaviors of porous metals under biaxial tensile loads," *Materials Science and Engineering: A*, vol. 422, no. 1-2, pp. 176–183, 2006.

[21] D. K. Shin, J. H. Yoo, D. G. Kang, and M. S. Kim, "Effect of cell size in metal foam inserted to the air channel of polymer electrolyte membrane fuel cell for high performance," *Renewable Energy*, vol. 115, pp. 663–675, 2017.

[22] W. Zhou, Q. Wang, J. Li et al., "Hydrogen production from methanol steam reforming using porous copper fiber sintered felt with gradient porosity," *International Journal of Hydrogen Energy*, vol. 40, no. 1, pp. 244–255, 2015.

[23] H. Meng, S. Ren, F. Xin, and T. Lu, "Sound absorption coefficient optimization of gradient sintered metal fiber felts," *Science China Technological Sciences*, vol. 59, no. 5, pp. 699–708, 2016.

[24] M. F. Ashby, A. G. Evans, N. A. Fleck, L. J. Gibson, and J. W. Hutchinson, *Metal Foams: A Design Guide*, Butterworth-Heinemann, Oxford, UK, 2000.

[25] O. B. Olurin, N. A. Fleck, and M. F. Ashby, "Joining of aluminium foams with fasteners and adhesives," *Journal of Materials Science*, vol. 35, no. 5, pp. 1079–1085, 2000.

[26] T. Bernard, H. W. Bergmann, C. Haberling, and H.-G. Haldenwanger, "Joining technologies for Al-foam-Al-sheet compound structures," *Advanced Engineering Materials*, vol. 4, no. 10, pp. 798–802, 2002.

[27] Y. Huang, J. Gong, S. Lv, J. Leng, and Y. Li, "Fluxless soldering with surface abrasion for joining metal foams," *Materials Science and Engineering: A*, vol. 552, no. 5, pp. 283–287, 2012.

[28] L. Wan, Y. Huang, T. Huang, Z. Lv, and J. Feng, "Interfacial behavior and mechanical properties of aluminum foam joint fabricated by surface self-abrasion fluxless soldering," *Journal of Alloys and Compounds*, vol. 671, pp. 346–353, 2016.

[29] J. Nowacki and K. Moraniec, "Evaluation of methods of soldering AlSi and AlSi-SiC particle composite Al foams," *Journal of Materials Engineering and Performance*, vol. 24, no. 1, pp. 426–433, 2015.

[30] A. A. Shirzadi, M. Kocak, and E. R. Wallach, "Joining stainless steel metal foams," *Science and Technology of Welding and Joining*, vol. 9, no. 3, pp. 277–279, 2013.

[31] T. Jarvis, W. Voice, and R. Goodall, "The bonding of nickel foam to Ti-6Al-4V using Ti-Cu-Ni braze alloy," *Materials Science and Engineering: A*, vol. 528, no. 6, pp. 2592–2601, 2011.

[32] U. Dilthey, A. Harms, and S. Longerich, "Joining strategies for open-porous metallic foams," *International Journal of Materials Research*, vol. 99, no. 4, pp. 359–366, 2006.

[33] W. Zhou, Y. Tang, M. Pan, X. Wei, and J. Xiang, "Experimental investigation on uniaxial tensile properties of high-porosity metal fiber sintered sheet," *Materials Science and Engineering: A*, vol. 525, no. 1-2, pp. 133–137, 2009.

[34] Y. Tang, W. Zhou, J. Xiang, W. Liu, and M. Pan, "An Innovative fabrication process of porous metal fiber sintered felts with three-dimensional reticulated structure," *Materials and Manufacturing Processes*, vol. 25, no. 7, pp. 565–571, 2010.